Plant–atmosphere heat exchange during wind machine operation for frost protection

Boekee, Judith; Dai, Yi; Schilperoort, Bart; van de Wiel, Bas J.H.; ten Veldhuis, Marie-Claire

DOI
10.1016/j.agrformet.2023.109312

Publication date
2023

Document Version
Final published version

Published in
Agricultural and Forest Meteorology

Agricultural and Forest Meteorology 330 (2023) 109312

Contents lists available at ScienceDirect

Agricultural and Forest Meteorology

journal homepage: www.elsevier.com/locate/agrformet

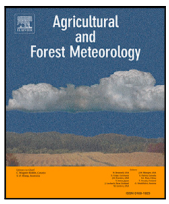

Plant–atmosphere heat exchange during wind machine operation for frost protection

Judith Boekee [a,*], Yi Dai [b], Bart Schilperoort [b,1], Bas J.H. van de Wiel [b], Marie-Claire ten Veldhuis [a]

[a] Delft University of Technology, Faculty of Civil Engineering and Geosciences, Department of Water Management, Stevinweg 1, 2628 CN, Delft, The Netherlands
[b] Delft University of Technology, Faculty of Civil Engineering and Geosciences, Department of Geoscience and Remote Sensing, Stevinweg 1, 2628 CN, Delft, The Netherlands

ARTICLE INFO

Keywords:
Agriculture
Frost mitigation
Leaf energy balance
Micro-meteorology
Wind machine

ABSTRACT

To mitigate spring frost damage, fruit farmers use wind machines to mix warm overlying air down to the vegetation. Up to this point, studies on wind machine efficiency have focused on air temperatures. The temperature of different plant organs during operation remains unknown, while critical for the actual degree of frost damage. With Distributed Temperature Sensing we measured vertical in-canopy air temperature profiles in a pear orchard in the Netherlands and thermistors were installed to determine the plant tissue temperatures. We found that to optimize wind machine operation, it is important to consider two effects of a wind machine: (1) mixing of stratified air above and into the canopy layer and (2) erosion of the leaf boundary layer to facilitate plant–air heat exchange. We show how foliage reduces plume penetration to the ground with distance to the wind machine. Due to this blocking at least 15 rotations (~ 75 min) are needed for optimal mixing. Leaf temperatures lag behind air temperatures, due to strong radiative cooling. We found that over the rotation cycle of a wind machine the temperature difference between leaf and air is variable as convective warming repeatedly dominates over radiative cooling. This is different for flowers and shoots due to different heat capacities. Thin flower petals store little heat and are almost in direct equilibrium with air temperature changes. Shoots, with their higher heat capacity and lower surface/volume ratio, store more heat during the day that is slowly released at night. This discrepancy between plant and air temperature should be considered for frost damage prediction.

1. Introduction

In many climates, spring frost can cause extensive damage to crops resulting in substantial economic losses in the agricultural sector (Snyder and Melo-Abreu, 2005). To mitigate this damage, farmers take measures to raise plant and air temperatures in their fields. Wind machines are increasingly used to prevent or mitigate the adverse effects of night frost, particularly in the fruit sector. Up to this point, studies on wind machine efficiency have focused on how wind machines change air temperatures. Here, we show how warm air aloft is transported into the canopy and subsequently warms plant leaves and flowers.

Wind machines prevent frost damage via two processes. Firstly, they mix the higher, warmer air with near-surface, colder air thus breaking the temperature inversion (Ribeiro et al., 2006; Battany, 2012). Secondly, they erode the viscous microscale boundary layer around the leaf surface, thereby enhancing the local heat transfer between (warmer) air and leaf (Snyder and Melo-Abreu, 2005; Kimura et al., 2017).

To decide when to turn on the wind machine, farmers monitor air temperatures to stay above a critical temperature range. The critical range is defined as the range of temperatures at which 10%–90% of the flower buds freeze and depends on the phenological development stage of the flower. As a flower develops from dormancy break to fruit set, the critical damage temperature increases (Quamme, 1978; Ashworth et al., 1989).

However, maintaining air temperature above the critical range does not ensure that damage is prevented. Critical temperature ranges are determined in a laboratory setting (in a so-called 'cold chamber') where plant and air temperatures are in equilibrium as a result of active mixing. In reality in the field, plant and air temperatures change at different rates. Especially in still air, plant tissue can be 1–3 degrees

* Corresponding author.
E-mail addresses: j.boekee@tudelft.nl (J. Boekee), y.dai-1@tudelft.nl (Y. Dai), b.schilperoort@gmail.com (B. Schilperoort), b.j.h.vandewiel@tudelft.nl (B.J.H. van de Wiel), j.a.e.tenveldhuis@tudelft.nl (J.A.E. ten Veldhuis).
[1] Present address: Netherlands eScience Center.

https://doi.org/10.1016/j.agrformet.2023.109312
Received 1 September 2022; Received in revised form 10 November 2022; Accepted 4 January 2023
Available online 17 January 2023

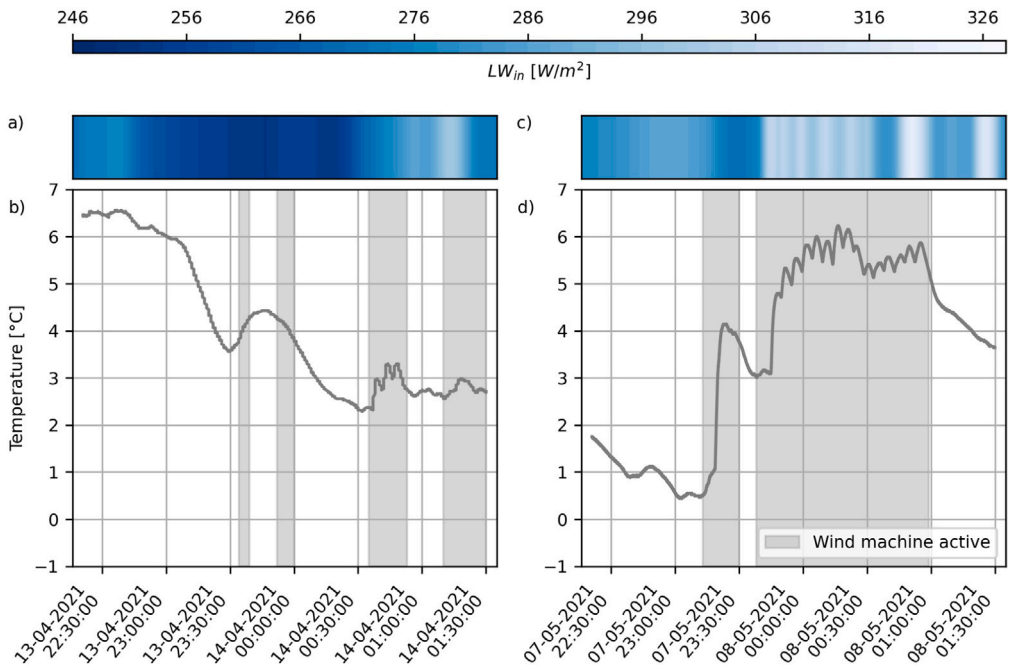

Fig. 1. Air temperature at 2 m height and incoming longwave radiation during the measurement nights in April (panel a & b) and May (panel c & d) at location N00-N, as indicated in Fig. 2.

cooler than the surrounding air (Landsberg et al., 1974; Leuning and Cremer, 1988; Monteith and Unsworth, 1990).

Plant–air energy exchange varies over a range of time scales (Monteith and Unsworth, 1990). Variations in micro-climate during frost events, such as wind speed and cloud cover, influence the temperature of plant tissue at short (minutes to hours) time scales (Perry, 1998). In-canopy air temperatures vary on longer timescales (hours to days) as a result of the bulk energy balance at the canopy–atmosphere interface (Dupont and Patton, 2012).

Previous work has explored the effect of wind machine operation modes on *air* temperatures in and above the canopy, with respect to tilt angle (Battany, 2012; Beyá-Marshall et al., 2019; Heusinkveld et al., 2020), rotation time (Heusinkveld et al., 2020) and timing of the start of machine operation (Ribeiro et al., 2006). Kimura et al. (2017) show how during the rotation cycle of a wind machine the *plant–air temperature difference* varies in a tea plantation. Using temperature measurements in artificial leaves distributed over the field, they find a delayed thermal response of the leaf. In fruit orchards, with a higher, more developed canopy, we expect an additional delay in temperature response to wind machine operation, due to stronger dampening by the canopy. Hence, to optimize wind machine operation in higher canopies such as fruit orchards, it is important to understand (1) how warm air mixes into the bulk canopy layer and (2) how the plant tissue responds to the induced fast fluctuations in micro-climate.

To answer these questions we use data from a field campaign in a pear orchard in Zeeland, The Netherlands during clear-sky nights in spring (Section 2). Using distributed temperature observations of the canopy air at high spatial resolution combined with leaf and flower bud temperatures, we study how warm air penetrates into the canopy. We use a conceptual model to quantify the energy exchange between plant and air during operation of the wind machine (Section 3). Conclusions and recommendations are considered in Section 4.

2. Materials and methods

2.1. Observations

2.1.1. Field site

Data were collected during field studies on 13–14 April 2021 and 7–8 May 2021 from approximately 20 h till 8 h, in a pear orchard in Krabbendijke (Zeeland, The Netherlands, 51°25'44.7"N, 4°8'8.5"E). The pear trees (variety: Pyrus communis L. 'Conference') are pruned to have 2–3 scaffold limbs and an open center. In April the trees are covered with buds and small leaves. In May the leaves are fully grown and only some late blossom is still present. The ground between the rows is covered with long grass and below the trees the bare soil is covered with mulch.

Since November 2018 this orchard is protected by a wind machine manufactured by Orchard-Rite®. The wind machine has a 10.7 m hub height and 6 m diameter double-bladed fan which blows air almost horizontally, with a modest downward angle of 8°. The blades rotate at 554 rpm, while the rotor makes a slow 360-degree rotation around its vertical axis, with a 5-min (user-specified) period. At a fixed location in the field, the passing of the jet can thus be experienced as a strong gust of relatively warm air. To limit the effect of 'statistical noise' data are phase-averaged over multiple rotations. This averaging is synchronized based on the moment where the peak in wind speed occurs, which receives timestamp zero.

The wind machine is activated automatically based on a critical temperature set by the farmer (1 °C at 1 m height) measured with an unshielded sensor. Nights for field observations are selected based on the calm wind conditions and (mostly) clear skies. An overview of the weather conditions in the field is presented in Fig. 1. On both nights the maximum wind speed observed at the nearby KNMI station in Woensdrecht (15 km to the West) is 1 m/s. In April, wind machine operation is intermittent for multiple short periods, due to fluctuating temperatures. In May, the wind machine makes two rotations after 23.30 h as the temperatures briefly fall below the critical temperature. At midnight, the wind machine is manually set to continuous mode to ensure continuous operation for one hour for the purpose of the field study.

2.1.2. Instruments

Fig. 2 shows an overview of the measurement set-up. High-resolution air temperature measurements are obtained through Distributed Temperature Sensing (DTS). This optical fiber technique uses the backscatter of a laser signal to infer local temperature at different cable sections with a sampling resolution of 25 cm and 10 s (Thomas

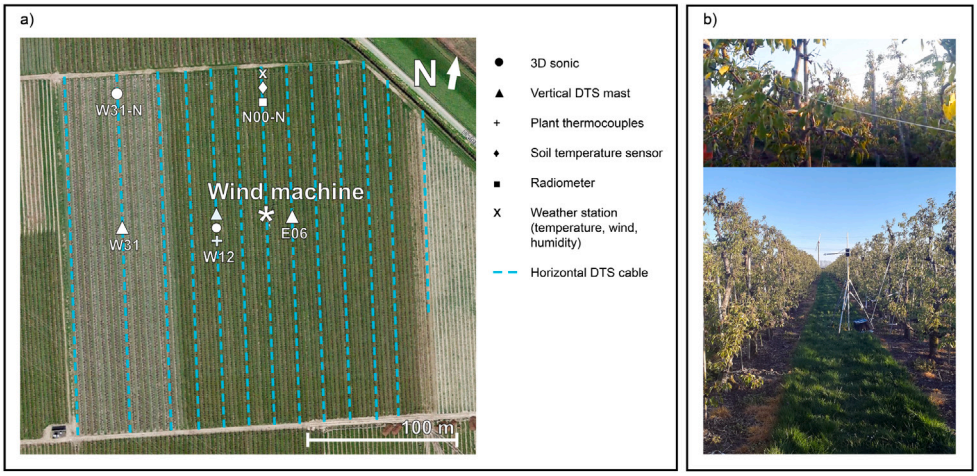

Fig. 2. Field set-up in the Krabbendijke orchard. Panel (a) shows the location of the different instruments. Symbols indicate the locations of the vertical DTS towers E06, W12 (only in May) and W31, 3D sonic-anemometers (only in May), soil temperature sensors, thermistors (only in May), HOBO weather station, and radiometer. The turquoise dotted lines are the horizontal DTS cables installed along the tree rows at 1 and 2 m height. Panel (b) shows the DTS cable (top) and the radiometer (bottom) during the May experiment.

et al., 2012). A thin 1.6 mm fiber optic cable and an Ultima-M system are used. A total cable length of 9 km is attached to the tree branches in a grid pattern to measure horizontal temperature variation at two heights. This is discussed in more detail in a separate paper by the same authors (Dai et al., 2022). In addition, 9 m high DTS towers are erected, at three locations relative to the machine: 12 rows West (~ 40 m distance, mast W12), 31 rows West (~ 110 m, mast W31), and 6 rows East (~ 20 m, mast E06). Two vertical cables are extended along each tower 1.5 m away from the trees.

In May the temperature of a tree close to mast W12 is monitored with small thermistors (Fig. 3). Each set of thermistors measured the temperature of the flower (T-Tissue, Ecomatik), shoot (T-Surface, Ecomatik), and leaf, as well as air temperature (LAT-B2, Ecomatik) at 2 cm from the leaf, at a temporal resolution of 0.1 Hz. The thermistors are pressed against the plant organs and thus measure the tissue surface temperature. Three sets of thermistors are installed at heights: 110 cm, 145 cm and 222 cm. Each set of thermistors is installed at the end of a new shoot, between 50 cm and 100 cm from the stem.

Radiation and soil temperatures are measured 100 m North of the wind machine (location N00-N). Soil temperature sensors (HOBO TMCx-HD) measure at 2, 5, 10 and 20 cm depth with a resolution of 5 min. A radiometer (Kipp & Zonen, CNR4) measures the incoming and outgoing short- and longwave radiation every minute. A HOBO weather station is installed at the same location, measuring wind speed and direction, air temperature, and humidity at 100 cm, 200 cm, and 300 cm height. Two sonic-anemometers (YOUNG Model 81000) are installed at W12 and W31-N, at 300 cm height, just above the canopy. Their measurement resolution is 10 Hz.

All processed data are available in the 4TU data repository, DOI: 10.4121/20581542.

2.2. Conceptual model

In this section, we present a conceptual model that enables us to investigate what processes drive plant–air heat exchange during wind machine operation. A similar modeling approach has been proven accurate for apple buds (Landsberg et al., 1974; Hamer, 1985, 1986) and blossom (Landsberg et al., 1974), and eucalyptus leaves (Leuning and Cremer, 1988; Leuning, 1988). The instantaneous plant–air temperature differences can be predicted with an error of less than 1 K, thus supporting our approach. We focus our analyses of air–plant heat exchange on the most vulnerable plant organs: leaves, flowers, and shoots. The energy balance of plant organs during a spring frost night is the sum of radiative cooling, turbulent warming, and latent heat release due to dew and ice formation (Monteith and Unsworth, 1990). As we observed no dew and ice formation during our field study, the latent heat release is considered negligible in our analyses.

The budget equation of a plant organ (i.e leaf, flower, or shoot) is therefore conceptualized here as:

$$C_{plant} * \frac{dT_{plant}}{dt} = R_N - H \quad (1)$$

in which R_N is the net radiation and H is convection in W/m^2 (Monteith and Unsworth, 1990). T_{plant} is the temperature of the plant tissue (i.e. leaf, shoot or flower) [K]. C_{plant} is the heat capacity per area of plant tissue [J m^{-2} K^{-1}].

2.2.1. Radiation

During the night net radiation is the sum of incoming and outgoing longwave radiation.

$$R_n = R_{lw,in} - R_{lw,out} \quad (2)$$

All surfaces surrounding plant tissue emit radiation: the sky, ground, and parts of the plant. A leaf hidden deep in the canopy receives a similar amount of longwave radiation from its neighbors as it is emitting itself. This results in radiative equilibrium. A leaf at the end of a shoot is exposed to the relatively cold sky and ground instead. It can thus cool down to below air temperature.

The longwave radiation emitted by a surface can be calculated through the Stefan–Boltzmann law:

$$R_{lw,out} = \sigma \varepsilon_{plant} T_{plant}^4 \quad (3)$$

in which ε is the emissivity and σ is Stefan–Boltzmann's constant [W m^{-2} K^{-4}].

The incoming longwave radiation $R_{lw,in}$ per square meter is a weighted average of incoming radiation from the canopy, sky, soil, and other plant tissue. The weighting factors are the fractions of the full hemisphere obscured by the different surfaces. This is the definition of the skyview factor SVF (Watson and Johnson, 1987). Here we also introduce the analogous ground view factor (GVF) and leaf view factor (LVF). Assuming a two-sided perfectly horizontal leaf (the lower half only faces the ground, and the upper half only faces clear or cloudy sky) gives:

$$R_{lw,in} = 0.5\mathrm{SVF}\sigma\varepsilon_{sky}T_{sky}^4 + 0.5\mathrm{GVF}\sigma\varepsilon_{soil}T_{soil}^4 + \mathrm{LVF}\sigma\varepsilon_{plant}T_{plant}^4 \quad (4)$$

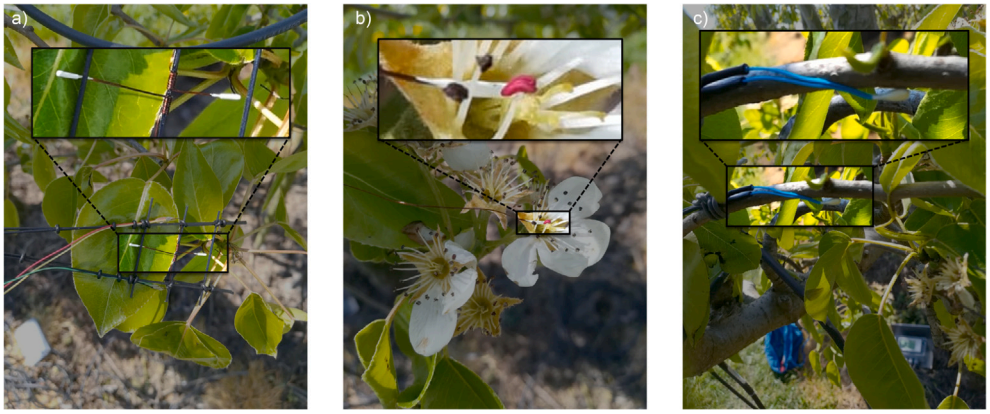

Fig. 3. Thermistors (leaf–air (panel a), flower (panel b), shoots (panel c)) installed in the orchard in Krabbendijke.

2.2.2. Convection

Turbulent mixing (H) between air and plant causes temperature differences to be reduced. H can be parameterized using a resistance law (Raschke, 1960):

$$H = \frac{\rho c_p \cdot (T_{plant} - T_{air})}{r_H} \tag{5}$$

here, ρ is the density [kg m^{-3}] and c_p heat capacity of air [J kg^{-1} K^{-1}].

r_H [s m^{-1}] is the resistance for turbulent heat transfer due to the presence of a leaf boundary layer. There are no universal relations that describe r_H. However, H can be non-dimensionalized as the Nusselt number (Schuepp, 1993):

$$\mathrm{Nu} = \frac{H/(\rho c_p)}{\kappa(T_{plant} - T_{air})/L} = \frac{L}{r_H \cdot \kappa} \tag{6}$$

here, L is the representative length scale of the leaf [m] and κ the thermal diffusivity of air [m^2 s^{-1}].

The Nusselt number is the ratio of convective to conductive heat transfer over a surface (or the ratio of 'turbulent' to molecular diffusivity). Its value depends on the local Reynolds number ($\mathrm{Re} = \frac{u \cdot L}{\nu}$) and local Grashof number ($\mathrm{Gr} = \frac{\left|T_{air}^{-1} \cdot g \cdot L^3 \cdot (T_{plant} - T_{air})\right|}{\nu^2}$). Here ν is the kinematic viscosity of the air [m^2/s], g the gravitational constant [m/s^2] and u the wind velocity [m/s]. Hence, we will use (universal) relations of the form $\mathrm{Nu} = f(\mathrm{Re}, \mathrm{Gr})$ in order to parameterize the turbulent heat flux. These universal flat-plate relationships have been adapted to approximate leaves in a natural environment. The formulations are given in Appendix A, Table A.1.

There are two modes of turbulent transport: "forced" convection (active) and "free" convection (passive). Forced convection is the exchange through the boundary layer of a surface exposed to a moving air stream, and free convection is the ascent/descent of warm/cold air over a surface due to density differences. Under forced convection Nu is therefore a function of the Reynolds number Re (ratio of inertial to viscous force). Under free convection, Nu depends on the Grashof number (ratio of buoyancy to viscous force).

Roth-Nebelsick (2001) and Bailey and Meneses (1995) motivated that purely free convection is unlikely to occur in nature, as even a very slight air movement already results in a significantly changed temperature distribution over a leaf surface. However, as highlighted by Schuepp (1993), the transition regime (i.e. "mixed" convection) is not uncommon in dense canopies or during lulls between stronger wind speeds. Interestingly, this is exactly what happens during wind machine operation. A leaf is alternatingly exposed to high wind conditions in which forced convection is dominant, and low wind conditions in which free convection plays a more important role. When both forced and free convection are important (i.e mixed convection), Nu is a function of both Re and Gr.

Finding a satisfactory description of the Nusselt number for mixed conditions remains a challenge. Generally, Nu is calculated for both forced and free convection and the largest value is used. Alternatively, forced and free conductances are summed, equivalent to parallel resistances (Schuepp, 1993).

The regime transitions between free, mixed and forced convection are often described in terms of (rigid) thresholds based on a so-called leaf-Richardson number Ri, defined as:

$$\mathrm{Ri} = \mathrm{Gr}/\mathrm{Re}^2 \tag{7}$$

As such it compares non-dimensional buoyancy effects over inertial effects. However, the exact Richardson borders for regime occurrence are not sharply defined (Parkhurst et al., 1968; Monteith and Unsworth, 1990).

Here, we introduce and apply a new conceptual view, that eliminates the need for empirical sharp boundaries between regimes. The logic of Eq. (7) can also be seen as the ratio of two competing Reynolds numbers, or likewise, as two competing velocity scales. This vision is explained in Appendix A. This reduces the need for the different formulations (Appendix A: Table A.1) to one equation, suitable for all quasi-laminar regimes ($\mathrm{Re}^* < 2 \cdot 10^4$):

$$\mathrm{Nu} = 0.6 \cdot (\mathrm{Re}^*)^{0.5} \tag{8}$$

and one for all turbulent regimes ($\mathrm{Re}^* > 2 \cdot 10^4$):

$$\mathrm{Nu} = 0.032 \cdot (\mathrm{Re}^*)^{0.8} \tag{9}$$

Here Re^* is the Reynolds number based on the refreshment velocity m^* that combines the wind velocity and a velocity scale for free convection:

$$m^* = \sqrt{(w^{free})^2 + u^2} \tag{10}$$

w^{free} is the typical velocity scale for free convection (Appendix A for derivation):

$$w^{free} = \sqrt{2Lg\frac{T_{plant} - T_{air}}{T_{air}}} \tag{11}$$

2.2.3. Model setup and calibration

Eq. (1) is solved numerically using an Euler forward method. We have tested for numerical convergence (and stability) for time steps between 0.001 and 10 s.

When we know the *volumetric* heat capacity of a plant organ [MJ m^{-3} K^{-1}], we can determine the heat capacity *per area* (C_{plant} in J m^{-2} K^{-1}). Therefore, we need to know the organ's shape, or at least the ratio between volume and surface area. We approximated the leaf and flower as flat circle-shaped plates with a thickness t_{plant} and radius L. The shoot was approached as a cylinder. Using typical heat volumetric capacities of 0.5, 2, and 4.2 MJ m^{-3} K^{-1} for respectively the flower, leaf,

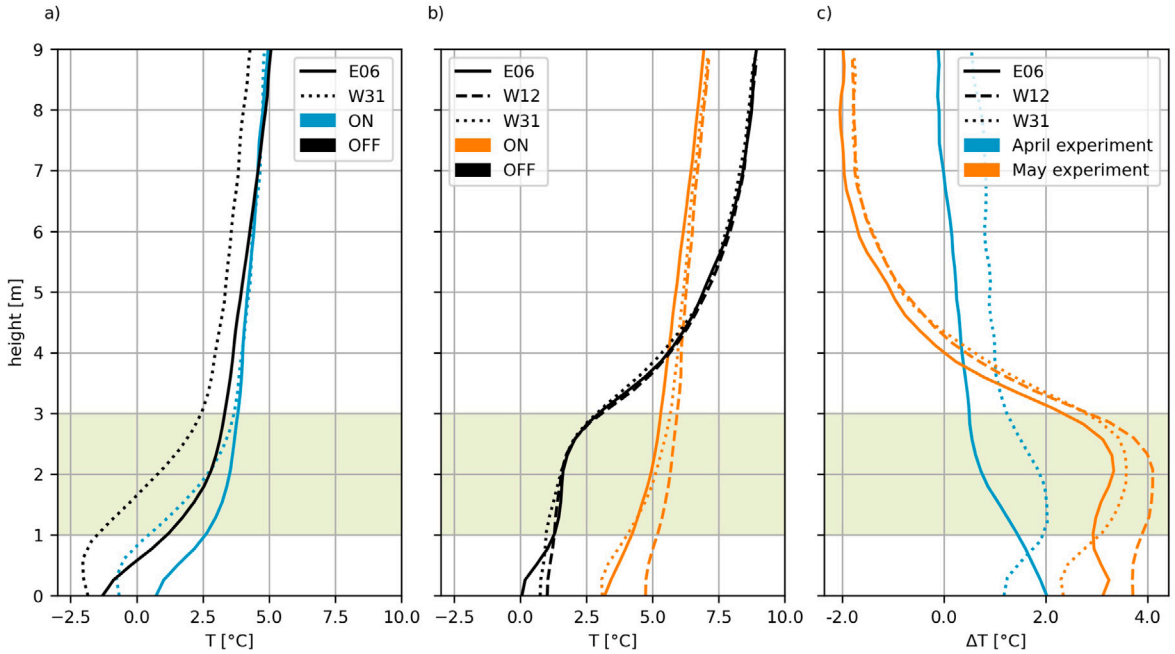

Fig. 4. Average temperature during ON and OFF mode of the wind machine, measured with the vertical DTS masts during April and May. Panel (a) shows April experiment, panel (b) May experiment, and panel (c) shows the *difference* between ON and OFF mode for both months. Green bars show the height of the horizontal shoots of the pear trees.

and shoot, we calibrated the thickness and radius. A number of realistic evenly spaced samples is taken for each parameter, and the modeled leaf temperatures are compared to the observations. The parameters that give the lowest MSE are selected. The exact values and calibration ranges are given in Appendix B, Table B.1.

The different plant parts also experience different SVFs and wind speeds due to the geometric effects of the canopy itself. This is included as $U_{plant} = \gamma * U_{obs}$, in which U_{plant} is the wind experienced by the plant, U_{obs} the observed wind at the top of the canopy and γ a height dependent constant between 0–1. As we did not measure the wind and radiation in the canopy, γ and SVF are also determined through calibration, resulting in a total of 5 calibration parameters for each of the three (flower, leaf, and shoot) models.

Note that the calibration parameters are indicative of the order of magnitude, and should not be interpreted as actual and exact values. For example, due to its turbulent character, wind can be quite different next to a leaf compared to just 5 cm distance. The model code is available on Github (https://github.com/judithboekee/blossom). It is intended for use only in combination with observation data for model tuning and verification.

3. Results and discussion

In this section, we first discuss how vertical temperature profiles in the bulk canopy layer respond to wind machine operation, at different locations and times in the growing season. Next, the energy transport between the leaf and atmosphere during the fast micro-climate fluctuations is quantified using observations in combination with the conceptual model outlined above.

3.1. Heat transport into the canopy

Vertical DTS cables measuring vertical temperature profiles are used to analyze heat transport into the canopy. Fig. 4 shows the mean vertical profiles during ON (14-04-2021 00:38 till 14-04-2021 00:50 and 07-05-2021 23:40 till 08-05-2021 01:00) and OFF (14-04-2021 00:00 till 14-04-2021 00:30 and 07-05-2021 22:30 till 08-05-2021 23:00) mode. Fig. 5 shows how these profiles vary over time during a phase-averaged rotation cycle.

In OFF mode, cooling of the overlying air by the cold surface results in a stable vertical temperature profile with the coldest temperatures and strongest vertical temperature gradient (i.e. a temperature inversion) close to the surface (Fig. 4a). In May the trees are leafed out and the inversion occurs at the top of the canopy at $z = 300$ cm instead of near the ground (Fig. 4b). Here the dense foliage cools radiatively. This limits the mixing of cold, dense air in the canopy with the warmer air above.

Interestingly, the rather uniform temperature within the canopy in the full leaf stage suggests that some kind of longwave radiative 'equilibrium' is reached, in absence of strong turbulent mixing. In accordance with Eqs. (2) and (3) this suggests that at each height within the canopy, LVF ≈ 1 (and SVF and GVF are approximately zero) and $R_{lw,in} \approx R_{lw,out}$.

In ON mode the vertical temperature gradient reduces. The operating wind machine accelerates air and generates a turbulent jet with an 8° downward angle. Flow instabilities at the edge of the jet (Kelvin–Helmholtz type) generate efficient mixing of in-canopy with the above-canopy air.

As a result, in the canopy, the air temperature rises. We observed an average temperature increase in the order of 1–3 °C near the ground. This is in line with earlier studies by Ribeiro et al. (2006) and Heusinkveld et al. (2020) who show an increase of ~ 2 °C. Above the canopy, the air temperature decreases. In May the temperature at 4–9 m height is lower during ON mode than during OFF mode (Fig. 4c). However, in April there is no cooling at this height. The above-canopy cooling was also not observed in January by Heusinkveld et al. (2020). We hypothesize that when there are no leaves on the trees, the mixing caused by the jet takes place over a rather deep layer exceeding hub height. However, there is no evidence from the current observations to confirm/falsify this.

Fig. 5 shows how the warm air aloft is mixed down into the canopy, far from the wind machine (Fig. 5a) and close by (Fig. 5c). The warm air first arrives above the canopy and penetrates between the trees as the wind speed increases. Interestingly, the highest temperature increase happens just *before* the maximum in the wind speed at $t = 0$. At W31 this takes about 60 s and at W12 about 30 s. The time difference is largest at the furthest location, which presumably is caused by plume

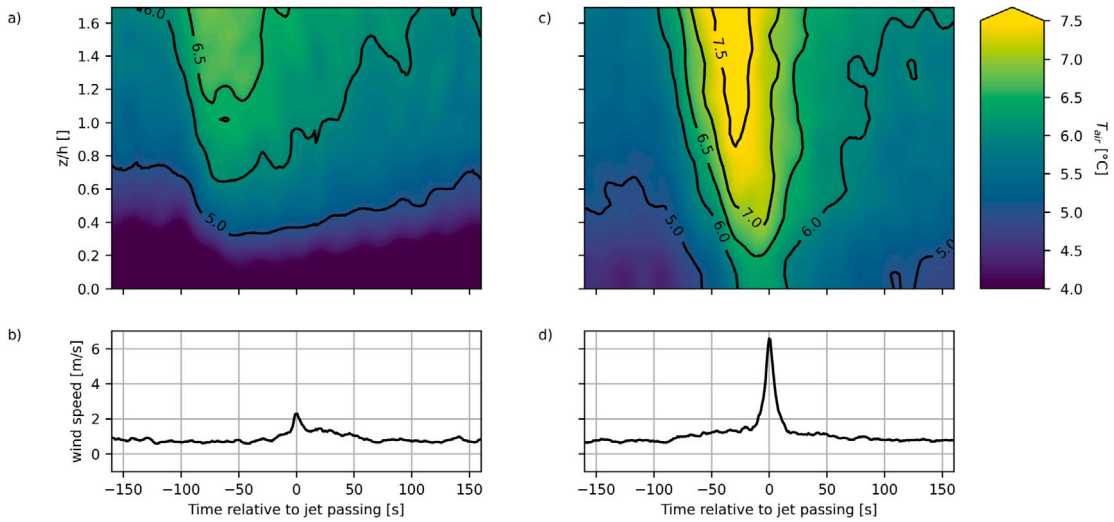

Fig. 5. The top panels (a, c) show average air temperatures as measured by the DTS cables in May in color and contour lines against height z/h, with canopy height h ~ 300 cm. The lower panels (b, d) show the averaged wind speeds as measured by the sonic anemometer just above the canopy. Panel (a) and (b) represent location W31 (~ 110 m) and panel (c) and (d) W12 (~ 40 m).

dispersion. This is explored more in-depth in a separate study on the same field experiment (Dai et al., 2022).

Next, we define a so-called plume penetration depth p_{plume}, to determine the influence of foliage density and radial distance from the wind machine on plume penetration. Penetration depth is defined as the normalized height below which the vertical temperature gradient remains larger than 0.5 K/m when the jet passes at $t = 0$. Below this height the effect of vertical mixing is limited. We define p_{plume} relative to the canopy height h, and is thus positive downwards into the canopy.

The mean temperature profiles during wind machine operation (Fig. 4) show that at the mast closest to the wind machine, the jet can penetrate completely to the ground (May, E06, ON mode). The penetration depth is $p_{plume} = 1$. The temperature gradient in the canopy is small: $dT/dz \sim 0.4$ K/m. At the location slightly further from the wind machine (May, W12, ON mode), only the upper half of the canopy air is well-mixed at $t = 0$. The penetration depth is $p_{plume} = 0.6$. For the location furthest from the fan (May, W31, ON mode), mixing of the in-canopy layer is suppressed. A significant temperature gradient of 0.8 K/m remains in the complete canopy layer, so the penetration depth $p_{plume} = 0$.

In April $p_{plume} = 0.5$ is at E06, at W31 $p_{plume} = 0$. In May the difference in penetration depth between the two masts is smaller. This is due to the increase in foliage density and difference in background conditions. In April a strong temperature inversion is present directly above the surface and minor turbulent mixing near the surface results in a strong temperature change. In May the vertical temperature gradient near the surface is smaller due to the presence of foliage and turbulent mixing will result in a comparatively smaller temperature change.

3.2. Heat transport from canopy air to leaf

To understand what is driving the energy exchange between leaf and air, we first diagnose the dominant mixing regimes. We use the classification given by Monteith and Unsworth (1990), which is based on the leaf-Richardson number in Eq. (7) and shown in Fig. 6a. The dominant regime is the 'Mixed convection' regime, followed by 'Forced convection' during passage of the wind machine jet. Occasionally, 'Free convection' occurs: in situations of very low wind speeds when the temperature difference between leaf and air is large. The wind speeds used for this classification are measured at the top of the canopy. The actual wind speeds next to the leaves will be lower and shifted towards free convection.

Fig. 6c shows how the plant tissue (i.e leaves) temperature responds to fluctuations in wind and air temperature. Directly after the first passage of the jet (start of the gray band in the figure) the air temperature 2 cm from the leaf rises by 5 degrees and this is followed almost instantly by the leaf temperature. Fig. 6d shows that leaves deeper in the canopy need more rotations to approach air temperature compared to those near the canopy top (222 cm). At the end of the active rotation period, air temperatures are the same at all heights in the canopy (not shown). All leaves have the same temperature as well, albeit 0.2 °C below the air temperature. From this, we conclude that the wind machine needs at least 15 rotations to reach maximum mixing in the canopy. This "warm-up" time is even more important for the vegetation, due to their delayed response compared to the air temperature. This is in line with the findings of Kimura et al. (2017), who show that boundary layer conductance is synchronized with wind machine oscillations, but leaf temperature reacts with a delay of several seconds.

3.3. Leaf energy balance

The conceptual model presented in Section 2.2 enables us to investigate what processes drive leaf–air heat exchange during wind machine operation. We introduced a refreshment velocity m^*, which combines the typical velocity scales for forced and free convection. By doing so we avoid the pre-imposed boundaries between turbulence regimes as used in Monteith and Unsworth (1990). In Fig. 7 we show how the aerodynamic resistances calculated using the original model (Monteith and Unsworth, 1990) result in a sharp change at $Ri = 10$, which is unlikely to exist in nature. We compare this to the m^*-based model which presents a more realistic gradual shift. Discrepancies between the two approaches occur mainly around the $Ri = 10$ boundary and over the range of very low velocities where Monteith and Unsworth (1990) assume the energy exchange through wind (i.e. forced convection) to be negligible. This causes discrepancies between the two approaches of up to 20%. Henceforth we use m^* in our model calculations.

The heat-exchange model is calibrated based on phase-averaged observations of air, soil, and sky temperature as input. Results of the predicted leaf temperature are given in Fig. 8a, together with the observations. The model reproduces the leaf temperature variation within an absolute error range of 0 to 0.2 °C, about 10% of the mean leaf–air temperature difference. Next, we use the model to compute the plant energy budget terms R_N and H, as shown in Fig. 8c.

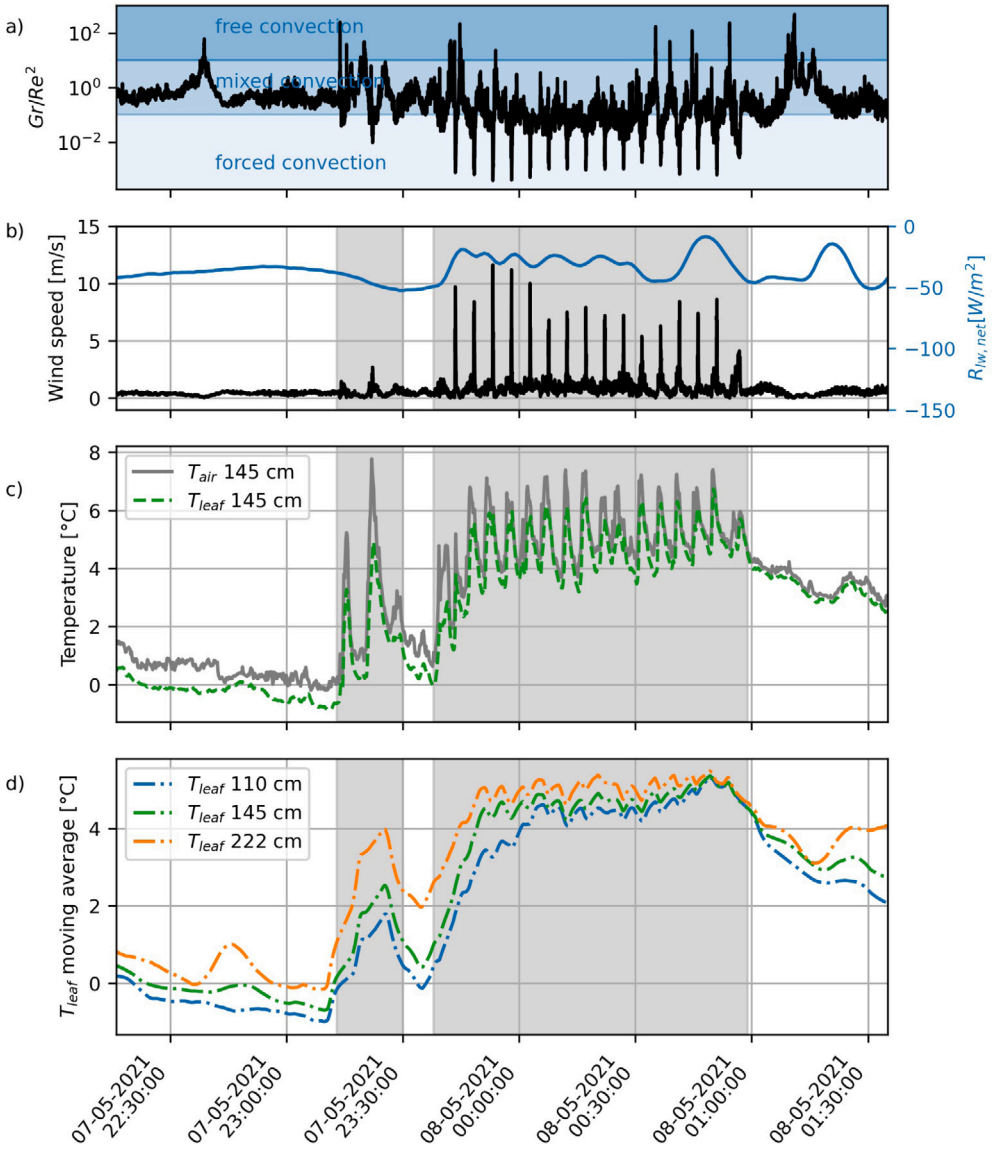

Fig. 6. Main mode of convective energy transport (i.e. according to criteria of Monteith and Unsworth (1990) in Table A.1) at 300 cm height (panel a). Wind speed and net longwave radiation (panel b), leaf and air temperature (panel c), and 500 s moving average of leaf temperature at three heights in the same tree to show the trend (panel d) before, during (highlighted in gray) and after operation of the wind machine in the night of 7–8 May at W12.

We divide the phase-averaged rotation cycle in three phases: the rising limb with a convex–concave shape, the temperature maximum, and the convex-shaped falling limb. As follows from Fig. 8c, the convective energy transport dominates during the first two phases, before and during the passage of the jet from $t = -150$ until $t = 10$. This corresponds to a strong increase in air temperatures (due to mixing of the in-canopy air) and thus a larger temperature difference between the air and the plant tissue. The convective heat flux increases linearly with the plant–air temperature difference and depends on the wind speed via the boundary layer resistance (Eq. (5)). Consequently, when the jet speed peaks at $t = 0$, the increase in wind speed enhances the convective energy exchange resulting in an additional leaf temperature increase of 0.2 K. After the passage of the peak (phase 3), radiative cooling again becomes dominant. At the start of phase 3, leaf temperature is nearly equal to the air temperature, the small temperature difference combined with low wind speeds limits further convective heat exchange. The leaf cools and radiative cooling gradually decreases. Finally, the influence of the next jet passage is felt (as the jet plume has a finite horizontal extent and is also advected), and convection rises again. Over the full rotation cycle, the heat introduced by convection was 1449 J/m^2 (area under H in Fig. 8c), 1416 J/m^2 (area under R_N in Fig. 8c) is lost due to radiative cooling. As long as the integrated convective warming is larger than the integrated radiative cooling the leaf will warm over time.

3.4. Different plant organs

Fig. 9 shows the averaged dynamic temperature response of leaves, flowers, and shoots to the passage of a wind machine jet. The flower tissue responds faster than the leaf due to its lower heat capacity and the difference between air and flower temperature remains close to zero (Fig. 9a). The flower temperature is measured at ~15 cm distance from the air temperature. This coherence in signal suggests that specific curve characteristics measured, such as the plateau at −150 to −100 s, have some general validity and are not a coincidence. The temperature response of a shoot differs from that of a leaf or flower: it warms and cools more slowly as a result of its smaller surface/volume ratio (Fig. 9a). We account for this by applying a higher heat capacity in the model, however, this results only in a delayed response as compared to the observational data (Fig. 9b, blue versus dashed curve). Moreover,

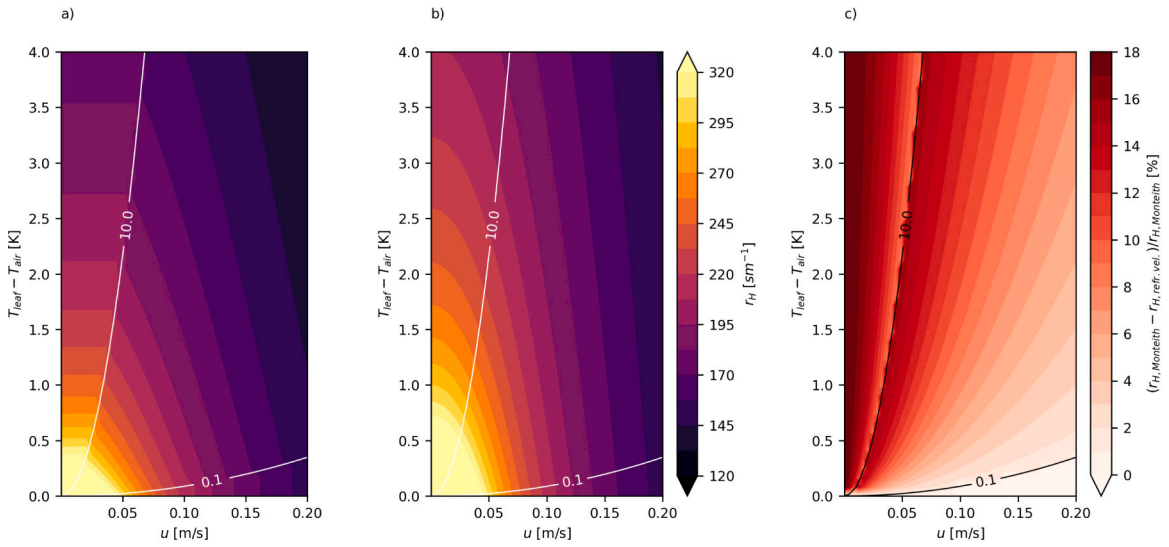

Fig. 7. Aerodynamic resistance r_H for a range of leaf temperatures and wind speeds, calculated using the approach presented by Monteith and Unsworth (1990) (panel a), and with our refreshment timescale (panel b), and the difference (panel c). Here we took $T_{air} = 273K$ and $L = 0.08m$ as typical values for the calculations.

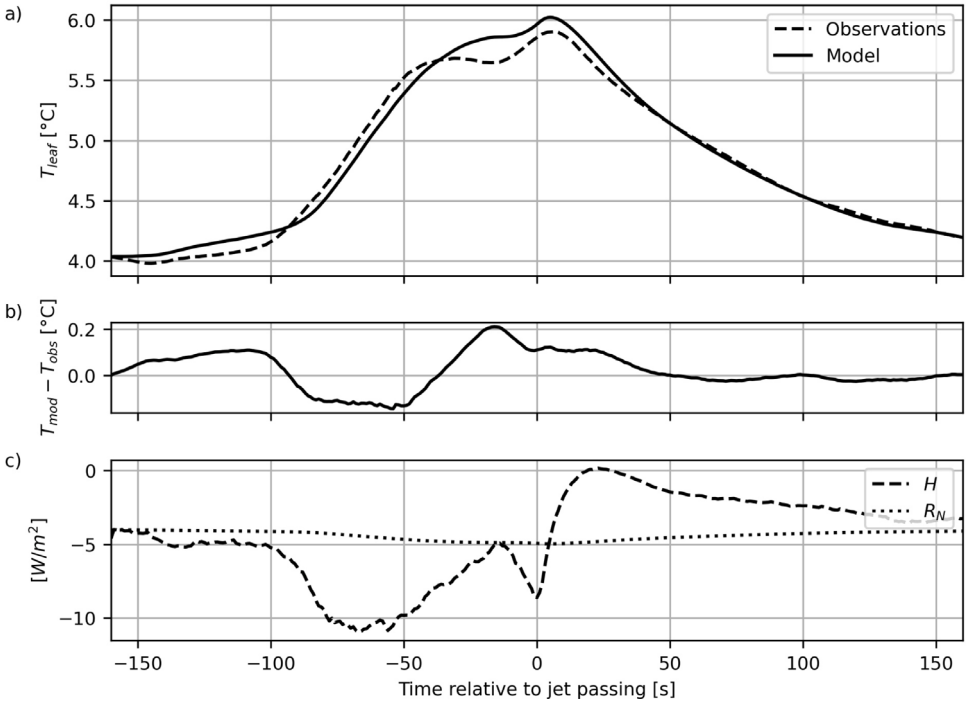

Fig. 8. Leaf temperature observed with the thermistors and model results (panel a) and the difference (panel b) over an averaged wind machine rotation at 145 cm height. Plant energy budget terms based on the observations according to Eq. (1): radiation (R_N), and forced and free convection (H) (panel c).

the model predicts an initial cooling (first 50 s) that is absent in the observations (Fig. 9b). This cooling computed by the model is a result of the air temperatures being below shoot temperature in combination with radiative cooling. On the contrary, in the observations, shoot temperature in the first 50 s remains almost constant. We hypothesize that cooling in the initial phase is counteracted by an (unknown) source of heat (or a delay process). We now empirically model this extra source of heat as a relaxation term in the budget equation:

$$S = \alpha \cdot (T_{core} - T_{shoot}) \tag{12}$$

in which, α is a constant, T_{core} is the temperature of the core of the shoot. As we did not measure this, we used the temperature of the soil at 20 cm depth, which was 8.8 °C. The physical meaning of the extra heat source is beyond the scope of this manuscript. Eq. (12) is fully empirical and could be interpreted as the heat release from the center of the shoot to its surface. This process works on a larger timescale and can be seen as delayed heat release from the day. In a separate analysis (not shown here) it was found that the shoot–air temperature difference decreased during wind machine operation. This indeed may suggest that heat storage effects on larger time scales may play a role here. The heat capacity C_{plant} in Eq. (1) does not cover this delayed heat release. It assumes instantaneous redistribution of heat through the plant tissue. For thin leaves and flowers, this is indeed the case. A thicker shoot or flower bud, however, has a frequency-dependent damping effect, similar to grass and soil (Van der Linden et al., 2022; Jacobs et al., 2008). Short term-variations in temperature, such as those caused by clouds or the passing of a wind machine jet, penetrate into the outer

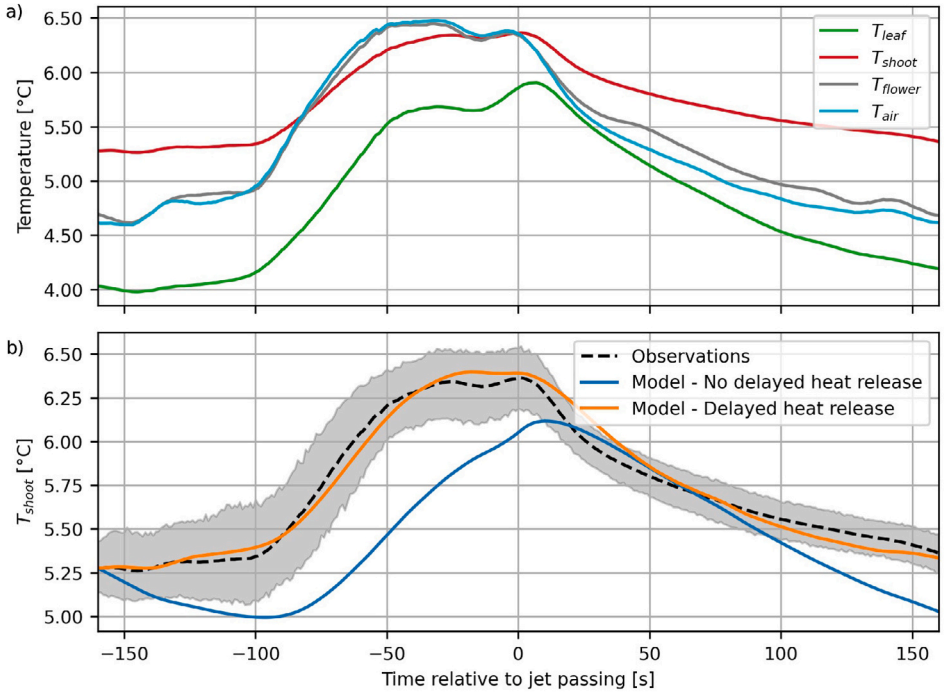

Fig. 9. Panel (a) shows all thermistor measurements at 145 cm: leaf, shoot, flower, and air temperatures. Thermistor sets at other heights show similar behavior. Panel (b) shows observed (the variation between the rotations shown by the gray band) and modeled temperature of the shoot, including (orange) and excluding (blue) a delayed heat release.

layer of the tissue only, but cannot reach the central part. Long-term temperature variations such as the diurnal cycle will penetrate to the core. These long-term variations will therefore have a significant effect on the temperature measured at the surface. With the inclusion of the extra heat source, which is promising in its simplicity, the model can accurately predict the dynamics of the shoot temperature.

4. Conclusion

In this study we investigate heat exchange processes in fruit tree canopies during wind machine operation. We deployed high-resolution Distributed Temperature Sensing (DTS) and leaf thermistors to measure temperature response of leaves, within-canopy and above-canopy air to the fast fluctuations in temperature and wind induced by the machine. We found that to optimize wind machine operation in fruit orchards, it is important to consider two effects of a wind machine: (1) mixing of stratified air above and into the canopy layer and (2) erosion of the leaf boundary layer to facilitate leaf–air energy exchange.

In addition to the average temperature increase, we looked at temperature variation over a five-minute rotation cycle. Thanks to the availability of high-resolution DTS data we are able to characterize the delayed response of in-canopy air temperature compared to the air above. Warm air arrives above the canopy just before the jet passes, due to plume dispersion. Due to plume dispersion, the above-canopy temperatures start rising before the jet core passes. Then, the stably stratified in-canopy air is mixed from the top down to a given penetration depth. This depth depends on the jet strength, distance to the wind machine and canopy density. We found penetration depths varying from 60% penetration close to the wind machine to 30% of the canopy at 110 m in early spring. Penetration was reduced with distance from full-canopy penetration to no penetration in late spring as a result of the denser foliage.

A second effect of the wind machine is erosion of the viscous boundary layer surrounding the leaves, flowers, and shoots by increased wind speeds. The same processes play a role here on the micro scale as on the canopy scale: convective warming and radiative cooling. Radiative cooling depends only on the temperature of the leaf and varies between −4 to −5 W/m^2. Preceding and during the passing of the jet convective energy exchange rises to 10 W/m^2 and dominates due to the high wind speed and large temperature difference. After the peak in wind speed, convective warming approaches zero and radiative cooling restores the temperature difference between air and plant. Before a new equilibrium temperature is reached, the next jet arrives and convective warming erodes the temperature difference again. As long as convective heat repeatedly introduced by the wind machine exceeds radiative cooling, the temperature of the plant tissue shows a positive trend over time, until equilibrium with the well-mixed canopy air is reached.

The conceptual energy balance model we use to quantify heat exchange between plant and air generally shows good agreement with the observations. Main deviations (up to 0.2 °C) occur just before jet passage, minor deviations are found during the rising limb of the temperature curve, as the jet approaches. The most likely explanation for these deviations is the position of wind observations used as input for the model. Sonic anemometers are installed above the canopy, because measuring representative 3D wind fields within a canopy is extremely challenging (Patton et al., 2011). We approximated wind speed in the canopy as a fraction of the wind on top of the canopy. In reality, the damping effect of the canopy is phase-dependent and changes the character of the flow by enhancing turbulence. To improve understanding of in-canopy energy exchange, measuring in-canopy wind velocities will be an important requirement. New developments in wind sensors like Freundorfer et al. (2021) and Alveringh et al. (2022) open a promising avenue for further research.

Our results show that temperature response of different plant organs depends on their heat capacity, strongly related to organ volume, and their surface/volume ratio. Thin flower petals store little heat and are almost in direct equilibrium (and synchronized) with air temperature changes. Leaves store small amounts of heat, but remain cooler than the air as convective warming is counterbalanced by strong radiative cooling. Shoots, with their higher heat capacity and lower surface/volume ratio, store more heat during the day which is slowly released at night. As a result, their temperature remains above air temperature, except

at passage of the wind machine, when air temperature briefly exceeds shoot temperature.

The focus of this study has been on temperature response of leaves and flower petals in fruit tree canopies. Our initial analyses of shoot temperature show that their response is significantly different from the thinner tissue of leaves and petals. We attribute this to the higher heat capacity resulting in larger heat storage during the day. This results in a higher average temperature and a dampened temperature response to wind jets in comparison to the leaves and flowers. By implementing a delayed heat release from the shoot core, we are able to replicate this effect with the model. However, to fully understand the origin of this delayed heat release, more observations and physics-based model efforts during wind machine operation are needed. Additional measurements of the internal temperature of the shoot, the stem and sap flow can support estimation of the heat transport from the core to the surface. Since flower buds are likely to show a similar dampened response and are the plant's most vulnerable organs in early spring, better understanding their temperature response is important for fruit frost protection.

Acknowledgments

The authors would like to thank Martijn Vogelaar of Vogelaar Fruitcultures for providing the experimental site. We thank Myrthe Breedijk, Rik Aulbers, Koen Harms, and Antoon van Hooft for their help during the field campaign. We also thank Harro Jongen for the fruitful discussions.

Funding

This work was supported by the NWO, The Netherlands [grant number ENWSS.2018.006].

Declaration of competing interest

The authors declare that they have no known competing financial interests or personal relationships that could have appeared to influence the work reported in this paper.

Appendix A. Parameterization of heat transfer: A conceptual background

The regime transitions between free and forced convection are often described in terms of (rigid) thresholds based on a Richardson criterion (Section 2.2), but are not sharply defined in literature. For example, Parkhurst et al. (1968) sets the limits for 5% departure from pure free or forced convection at $0.1 < \mathrm{Ri} < 16$. Monteith and Unsworth (1990) states that mixed convection is probable for $0.1 < Ri < 10$. As such the 'threshold' are mere indicators of transition based on empirical evidence and they will vary strongly with the dimensions of the plant surface and the turbulent conditions of the air. Table A.1 shows an example of how the Richardson number can be used to define boundaries between the different convection regimes, and how the Nusselt number is parameterized for those different scenarios. In reality, regime transitions are more smooth.

As a simpler alternative that allows for a more smooth (i.e. more natural) transition between the regimes, here we present a conceptual picture based on a mechanistic approach. By introducing a free-convection type of velocity scale, we show how the Nusselt number can be calculated directly as to avoid the use of different formulations in the free and forced convection regime.

A.1. Free convection velocity scale

In a situation with no background wind, air movement results from the air density difference between the relative warm/cold air above the leaf surface and the surrounding air (i.e free convection). The *apparent* gravity force g^* on an air parcel over a leaf surface can be calculated by correcting the gravity force F_g for the buoyant force F_B [N]:

$$F_g = F_B \tag{A.1}$$

$$\rho_{air} V a = (\rho_{plant} - \rho_{air}) V g \tag{A.2}$$

where ρ_{air} is the density of air outside of the leaf boundary layer [kg m^{-3}], V is the volume of an air parcel [m^3] and a is its acceleration [m s^{-2}]. ρ_{plant} is the air density within the leaf boundary layer, and g is the gravitational acceleration of 9.81 m s^{-2}. This gives the apparent gravity g^* [m s^{-2}].

$$g^* = a = g\frac{\rho_{plant} - \rho_{air}}{\rho_{air}} = g\frac{T_{plant} - T_{air}}{T_{air}} \tag{A.3}$$

The typical velocity scale w^{free} for free convection can then be derived from the apparent gravity and the typical length scale L ($L = \frac{1}{2}g^*t^2$):

$$w^{free} = tg^* = \sqrt{2Lg^*} \tag{A.4}$$

When we take the squared ratio of the buoyant velocity scale to the wind speed, we notice that this is equal to twice the Richardson number.

$$\left(\frac{w^{free}}{u}\right)^2 = \frac{2Lg^*}{u^2} = \frac{\frac{g \cdot L^3 \cdot \frac{(T_{plant} - T_{air})}{T_{air}}}{\nu^2}}{\left(\frac{uL}{\nu}\right)^2} = \frac{2Gr}{Re^2} = 2Ri \tag{A.5}$$

So, this suggests that the Grashof number can also be seen as the square of a characteristic Reynold number for w^{free}. This vision can be appreciated from Table A.1 where the powers in the Grashof formulations are roughly half of the Reynolds powers. As such, instead of using the *different* parametrizations for Nu based on Re and Gr, we introduce a parameterization based on a *single* Reynolds number. To this end, we will base Reynolds number Re^* on the refreshment velocity m^*, which combines the background velocity and w^{free}.

$$m^* = \sqrt{(w^{free})^2 + u^2} \tag{A.6}$$

This new view reduces the need for the different formulations (Table A.1) to one equation, suitable for all quasi-laminar regimes ($\mathrm{Re}^* < 2 \cdot 10^4$):

$$\mathrm{Nu} = 0.6 \cdot (\mathrm{Re}^*)^{0.5} \tag{A.7}$$

and one for all turbulent regimes ($\mathrm{Re}^* > 2 \cdot 10^4$):

$$\mathrm{Nu} = 0.032 \cdot (\mathrm{Re}^*)^{0.8} \tag{A.8}$$

Here we select the original parameterization for laminar and turbulent flow. Perhaps, the complexity could be further reduced when both regimes are merged into a single formulation for all Reynolds regimes. This follows from the fact that the lower coefficient in Eq. (A.8) is partly compensated by a higher power. However, designated laboratory experiments are needed in order to investigate this from a parameter perspective. Here we restrict ourselves to the conceptual view, rather than to finding the most optimal parameters.

Finally, we notice that in the analysis aspects of branch and leaf vibration as a result of the wind are not taken into account explicitly. In reality however, those effects are likely to be important. Below, it will be motivated that those physical effects do have an effect on the characteristic length scale choices made.

Table A.1
Original flow regime criteria given in Monteith and Unsworth (1990) as to calculate the Nusselt number under different conditions. Where the table is based on rigid criteria, here a more smooth alternative is given.

			Nu=
Free convection	Ri>10	$T_{plant} <= T_{air}$	$0.13 \cdot Gr^{0.33}$
		$T_{plant} > T_{air}$	$0.50 \cdot Gr^{0.25}$
Forced convection	Ri<0.1	$Re <= 2 \cdot 10^{-4}$	$0.60 \cdot Re^{0.5}$
		$Re > 2 \cdot 10^{-4}$	$0.32 \cdot Re^{0.8}$
Mixed convection	0.1<Ri<10		$\left(Nu_{free}^{3.5} + Nu_{forced}^{3.5}\right)^{1/3.5}$

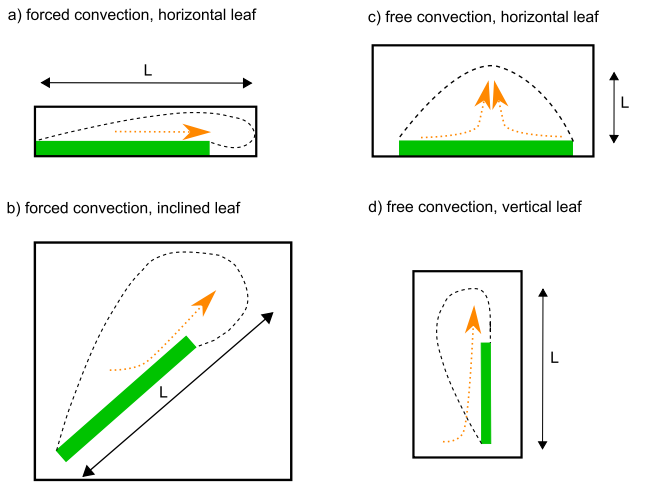

Fig. A.1. Different scenarios for flow along a leaf. Panel (a) and (b) show forced convection scenarios with horizontal or inclined leaf. Panel (c) and (d) show free convection for horizontal or vertical leaves. The orange arrow illustrates a possible flow path. While the black arrow illustrates a typical length scale.

A.2. Typical length scale

Note that due to every flower's, leaf's or shoots' unique shape it is hard to define a typical length scale used to calculate w^{free}. For a sphere, cylinder or flat plate the diameter or length in the direction of the wind would be a logical choice. For an irregularly shaped leaf fluttering in the wind, the characteristic dimension L can be anything between the thickness and the maximum length of the leaf. We expect typical length scales to be between 0.5–0.8 times the maximum leaf dimension (Parkhurst et al., 1968; Schuepp, 1993). Fig. A.1 shows three different scenarios to explain this statement. During conditions of forced or mixed convection, there is a slight background wind, and leaves are usually streamlining along the flow, like in Fig. A.1a (though often vibrating as well). For leaves that are not streamlining, anabatic effects and flow detachment will start to play a role, elongating the acceleration time (Fig. A.1b). For situations of no flow, Kitamura et al. (2015) and Graefe et al. (2022) show that for respectively horizontal (Fig. A.1c) or (vertically) inclined leaves (Fig. A.1d), the typical length is chosen along the steepest ascent of the leaf surface and thus also in the order of magnitude of the leaf length. For this reason in the analysis above the maximum leaf length is taken as the characteristic length scale (rather than e.g. leaf thickness).

Appendix B. Model iteration parameters

The values for the typical length scale and thickness should be interpreted with care. They do not represent the actual shape of the plant organ, but are used to determine the surface/volume ratio and are representative of the typical length scale (see also Appendix A).

Table B.1
Parameters used for modeling the plant tissue temperature. Exact values of constant α [–], thickness of the plant organ t_{plant} [mm], representative length scale L [mm], Sky View Factor SVF [–] and wind reduction factor γ [–] were determined through calibration within the given range [minimum.. maximum, number of evenly spaced samples]. ε is the emissivity [–] (same for all organs) and c_p is the heat capacity of the plant tissue [J kg^{-1} K^{-1}].

	Shoot	Leaf	Flower	Calibration range
α	22			[0..50; # = 10]
t_{plant}		0.2	0.12	[0.1..1, # =10] for leaf [0.01..1, # = 10] for flower
L	1.2	40	3.4	[0.1..10, # = 10] for shoot [10..100, # = 10] for leaf [0.1..10, # = 10] for flower
SVF	1	0.1	0	[0..1 , # = 11]
γ	1	0.8	1	[0..1 , # = 11]
ε_{air}	0.8			
ε_{plant}	0.96			
ε_{soil}	0.98			
c_{plant}	$4.2 \cdot 10^6$	$2.0 \cdot 10^6$	$0.5 \cdot 10^6$	

References

Alveringh, D., Bijsterveld, D.G., van den Berg, T.E., Veltkamp, H.W., Batenburg, K.M., Sanders, R.G.P., Lotters, J.C., Wiegerink, R.J., 2022. A miniature microclimate thermal flow sensor for horticultural applications. In: Proceedings of the IEEE SENSORS Conference. http://dx.doi.org/10.1109/SENSORS52175.2022.9967348.

Ashworth, E., Davis, G.A., Wisniewski, M.E., 1989. The formation and distribution of ice within dormant and deacclimated peach flower buds. Plant Cell Environ. 12, http://dx.doi.org/10.1111/j.1365-3040.1989.tb02125.x.

Bailey, B., Meneses, J., 1995. Modelling leaf convective heat transfer. ISHS Acta Hortic. 399, 191–198. http://dx.doi.org/10.17660/ActaHortic.1995.399.22.

Battany, M.C., 2012. Vineyard frost protection with upward-blowing wind machines. Agric. For. Meteorol. 157, 39–48. http://dx.doi.org/10.1016/j.agrformet.2012.01.009.

Beyá-Marshall, V., Herrera, J., Santibáñez, F., Fichet, T., 2019. Micro-climate modification under the effect of stationary and portable wind machines. Agric. For. Meteorol. 269, 351–363. http://dx.doi.org/10.1016/j.agrformet.2019.01.042.

Dai, Yi, Boekee, Judith, Schilperoort, Bart, ten Veldhuis, Marie-Claire, van de Wiel, Bas, 2022. Wind machines for frost damage mitigation: a quantitative 3d investigation based on observations. Available at SSRN 4248324 (in review).

Dupont, S., Patton, E.G., 2012. Influence of stability and seasonal canopy changes on micrometeorology within and above an orchard canopy: The chats experiment. Agric. For. Meteorol. 157, 11–29. http://dx.doi.org/10.1016/j.agrformet.2012.01.011.

Freundorfer, A., Lapo, K., Schneider, J., Thomas, C.K., 2021. Distributed sensing of wind direction using fiber-optic cables. J. Atmos. Ocean Technol. 38, 1871–1883. http://dx.doi.org/10.1175/JTECH-D-21-0019.1.

Graefe, J., Grosch, R., Bitterlich, M., 2022. The boundary layer conductance of inclined elliptical leaves under free convection. Agric. For. Meteorol. 317, 108884. http://dx.doi.org/10.1016/j.agrformet.2022.108884.

Hamer, P., 1985. The heat balance of apple buds and blossoms. Part I. Heat transfer in the outdoor environment. Agric. For. Meteorol. 35, 339–352. http://dx.doi.org/10.1016/0168-1923(85)90094-2.

Hamer, P., 1986. The heat balance of apple buds and blossoms. Part II. The water requirements for frost protection by overhead sprinkler irrigation. Agric. For. Meteorol. 37, 159–174. http://dx.doi.org/10.1016/0168-1923(86)90006-7.

Heusinkveld, V.W., van Hooft, J.A., Schilperoort, B., Baas, P., van de Wiel, B.J., et al., 2020. Towards a physics-based understanding of fruit frost protection using wind machines. Agric. For. Meteorol. 282, 107868. http://dx.doi.org/10.1016/j.agrformet.2019.107868.

Jacobs, A.F., Heusinkveld, B.G., Holtslag, A.A., 2008. Towards closing the surface energy budget of a mid-latitude grassland. Boundary-Layer Meteorol. 126, 125–136. http://dx.doi.org/10.1007/s10546-007-9209-2.

Kimura, K., Yasutake, D., Nakazono, K., Kitano, M., 2017. Dynamic distribution of thermal effects of an oscillating frost protective fan in a tea field. Biosyst. Eng. 164, 98–109. http://dx.doi.org/10.1016/j.biosystemseng.2017.09.010.

Kitamura, K., Mitsuishi, A., Suzuki, T., Kimura, F., 2015. Fluid flow and heat transfer of natural convection adjacent to upward-facing, rectangular plates of arbitrary aspect ratios. Int. J. Heat Mass Transfer 89, 320–332. http://dx.doi.org/10.1016/j.ijheatmasstransfer.2015.05.075.

Landsberg, J., Butler, D., Thorpe, M., 1974. Apple bud and blossom temperatures. J. Hortic. Sci. 49, 227–239. http://dx.doi.org/10.1080/00221589.1974.11514574.

Leuning, R., 1988. Leaf temperatures during radiation frost Part II. A steady state theory. Agricult. Forest Meteorol. 42, 135–155. http://dx.doi.org/10.1016/0168-1923(88)90073-1.

Leuning, R., Cremer, K., 1988. Leaf temperatures during radiation frost part I. Observations. Agric. For. Meteorol. 42, 121–133. http://dx.doi.org/10.1016/0168-1923(88)90072-X.

Monteith, J., Unsworth, M., 1990. Principles of Environmental Physics: Plants, Animals, and the Atmosphere. Academic Press, http://dx.doi.org/10.1016/C2010-0-66393-0.

Parkhurst, D., Duncan, P., Gates, D., Kreith, F., 1968. Wind-tunnel modelling of convection of heat between air and broad leaves of plants. Agric. Meteorol. 5, 33–47. http://dx.doi.org/10.1016/0002-1571(68)90021-6.

Patton, E.G., Horst, T.W., Sullivan, P.P., Lenschow, D.H., Oncley, S.P., Brown, W.O., Burns, S.P., Guenther, A.B., Held, A., Karl, T., et al., 2011. The canopy horizontal array turbulence study. Bull. Am. Meteorol. Soc. 92, 593–611. http://dx.doi.org/10.1175/2010BAMS2614.1.

Perry, K.B., 1998. Basics of frost and freeze protection for horticultural crops. Hort. Technol. 8, 10–15. http://dx.doi.org/10.21273/HORTTECH.8.1.10.

Quamme, H.A., 1978. Mechanism of supercooling in overwintering peach flower buds. J. Am. Soc. Hortic. Sci. 103.

Raschke, K., 1960. Heat transfer between the plant and the environment. Annu. Rev. Plant Physiol. 11, 111–126. http://dx.doi.org/10.1146/annurev.pp.11.060160.000551.

Ribeiro, A.C., De Melo-Abreu, J.P., Snyder, R.L., 2006. Apple orchard frost protection with wind machine operation. Agric. For. Meteorol. 141, 71–81. http://dx.doi.org/10.1016/j.agrformet.2006.08.019.

Roth-Nebelsick, A., 2001. Computer-based analysis of steady-state and transient heat transfer of small-sized leaves by free and mixed convection. Plant Cell Environ. 24, 631–640. http://dx.doi.org/10.1046/j.1365-3040.2001.00712.x.

Schuepp, P., 1993. Tansley review (59) leaf boundary layers. New Phytol. 477–507. http://dx.doi.org/10.1111/j.1469-8137.1993.tb03898.x.

Snyder, R.L., Melo-Abreu, J.d., 2005. Frost Protection: Fundamentals, Practice and Economics, Vol. 1. http://dx.doi.org/10.1017/s0014479706273794.

Thomas, C.K., Kennedy, A.M., Selker, J.S., Moretti, A., Schroth, M.H., Smoot, A.R., Tufillaro, N.B., Zeeman, M.J., 2012. High-resolution fibre-optic temperature sensing: A new tool to study the two-dimensional structure of atmospheric surface-layer flow. Boundary-Layer Meteorol. 142, 177–192. http://dx.doi.org/10.1007/s10546-011-9672-7.

Van der Linden, S., Kruis, M.T., Hartogensis, O., Moene, A.F., Bosveld, F.C., van de Wiel, B.J., 2022. Boundary-layer meteorology heat transfer through grass : A diffusive approach. Boundary-Layer Meteorol. 184, 251–276. http://dx.doi.org/10.1007/s10546-022-00708-7.

Watson, I., Johnson, G., 1987. Graphical estimation of sky view-factors in urban environments. Int. J. Climatol. 7, 193–197. http://dx.doi.org/10.1002/joc.3370070210.